Investigation of Properties of Mg n Clusters and Their Hydrogen Storage Mechanism: A Study Based on DFT and a Global Minimum Optimization Method

ARTICLE *in* THE JOURNAL OF PHYSICAL CHEMISTRY A · MARCH 2015

Impact Factor: 2.69 · DOI: 10.1021/acs.jpca.5b01474 · Source: PubMed

5 AUTHORS, INCLUDING:

Ran Jia

Technische Universität München

29 PUBLICATIONS **112** CITATIONS

SEE PROFILE

THE JOURNAL OF PHYSICAL CHEMISTRY A

Article

pubs.acs.org/JPCA

Investigation of Properties of Mg_n Clusters and Their Hydrogen Storage Mechanism: A Study Based on DFT and a Global Minimum Optimization Method

Dong Shen, Chui-Peng Kong, Ran Jia, Peng Fu, and Hong-Xing Zhang*

Institute of Theoretical Chemistry, State Key Laboratory of Theoretical and Computational Chemistry, Jilin University, Changchun 130023, People's Republic of China

Supporting Information

ABSTRACT: The global minimum structures of Mg_n clusters have been determined using the so-called "kick method". With the improved DFT method of B3PW91 functional and Grimme's dispersion correction, a series of the most stable structure of Mg_n have been found and a novel Mg_9 structure has been located. Subsequently, the chemisorption of hydrogen onto Mg clusters was systemically studied. Considering the average adsorption energies and the ratio of Mg and H, we developed a function that can describe the relation between average adsorption energy and number of Mg and H atoms. Our results may be helpful in the future for developing different kinds of gas chemisorption materials.

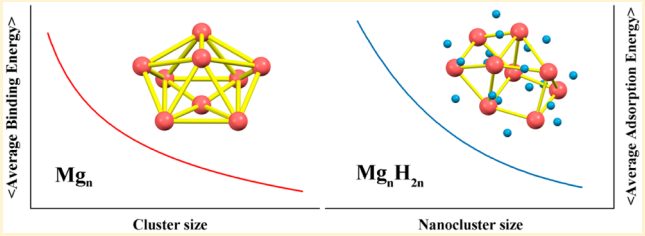

1. INTRODUCTION

With increasing energy consumption and the air pollution problem, fossil fuels are gradually being replaced by renewable energy sources. Among the various energy resources, hydrogen may become one of the most promising because of its higher energy density, environmental friendliness, inexhaustible reserve, and high efficiency.[1] During the application of hydrogen energy, a crucial issue which influences the hydrogen utilization is the development of cost-effective hydrogen storage carriers.[2−4] In order to solve this problem, various kinds of hydrogen storage schemes have been presented. The most efficient approaches are to store it in gas or liquid state. However, hydrogen storage in gas or liquid state usually requires low temperature and high pressure. Thus, a new hydrogen storage method is still worth studying.

Nowadays, most of the research focuses on the solid or liquid state hydrogen storage materials which have many advantages like high capacity, high safety, and low cost. The hydrogen storage material can be classified into two categories—physisorption (carbon materials,[5] metal organic framework,[6,7] etc.) and chemisorption (metal,[8−11] complex hydride,[12,13] organic hydride,[14,15] etc.). According to previous studies, inorganic compounds, such as $LaNi_5$,[9] $LiBH_4$,[4] and $NaAlH_4$,[6] may become a kind of prominent hydrogen storage material due to their high energy density, high stability, and low costs.

Among all kinds of metallic materials, Mg is one of the most promising hydrogen storage materials due to its high storage capacity of 7.69 wt %,[2,16] abundant reserve, and low cost. However, the slow absorption or desorption kinetics and high operating temperatures (350−400 °C) limit the applications of Mg-based materials.[2] By both theoretical[17,18] and experimental[19−24] evidence, one of the solutions is to reduce the size of the Mg particles to the nanoscale. This can improve the thermodynamic and kinetic properties of hydrogen absorption and desorption, because of the large surface area, short diffusion length,[20] and nanostructured phase[23,24] in nano-Mg particles. Recently, Jeon et al. have prepared a composite that contains more than 60 wt % of nano-Mg particles. It can adsorb and release hydrogen rapidly below 200 °C.[22] In addition, Schimmel et al. also have found that there may exist a nanostructured phase of MgH_x ($x < 2$) in a ball-milled nanostructure of MgH_2[24] and the hydrogen can diffuse much more rapidly in this phase.[23] Although many relative studies have been made in the past, the detailed structure and hydrogen storage mechanism of the Mg nanoparticles remains to be studied.

In this study, we use the so-called "kick method"[25−27] to obtain the global minimum state of the Mg_n cluster. On this basis, the hydrogen is added gradually to the Mg_n cluster a pair of atoms at a time, obtaining the Mg_nH_{2m} nanocluster. This process is repeated up to Mg_nH_{2n+2}. In previous theoretical studies, both the Mg_n cluster and the Mg_nH_{2m} (or MgH_2, Mg_nH_{2n}) nanocluster are calculated at density functional theory (DFT).[17,18,28,29] While in this study, the van der Waals correction is considered with the Grimme's dispersion (D3). According to the calculations of Mg_n clusters, we find a more stable Mg_9 cluster comparing to previous work.[28,29] Moreover, we obtain the relationship between average binding energies of Mg_n clusters and cluster size. In Mg_nH_{2m} nanocluster calculations, we attempt to construct the dependence of

Received: February 12, 2015
Revised: March 23, 2015
Published: March 24, 2015

DOI: 10.1021/acs.jpca.5b01474
J. Phys. Chem. A 2015, 119, 3636−3643

average adsorption energies of Mg_nH_{2m} clusters on size (n) and composition (m).

2. COMPUTATIONAL METHODS

2.1. Calculation Methods. All the calculations in this study were performed with the *Gaussian 09* software package (D.01 version). The density functional theory (DFT) method[30,31] was applied to balance the cost and accuracy of computation. According to previous publications and our own test[28] (see Supporting Information, Table S6), we employ the hybrid Becke-type three-parameter exchange functional[32] paired with the gradient-corrected Perdew−Wang 91 correlation functional[33] (B3PW91). In order to include the van der Waals interaction between magnesium atoms,[28] the Grimme's dispersion correction (DFT-D3)[34] was applied.

The global minimum state for each Mg_n cluster is determined with the "kick method".[25−27] For each Mg_n cluster (n = 2−17), an initial structure is generated with all the atoms placed randomly within a sphere of a certain diameter. After that, this random structure is optimized with the basis set at the 6-31G(d) level with the subsequent calculation of frequencies. In our study, 50 structures are obtained and compared in total. Then, the global minimum state of the cluster is selected as the structure with the lowest energy and without imaginary frequencies.[35] At last, the structure obtained at the 6-31G(d) level is further optimized in turn with 6-311+G(d,p) and the aug-cc-pVDZ basis set (including the calculation of frequencies) so as to obtain the relatively accurate structure and energy for each Mg_n cluster.

Finding the ground state geometry of Mg_nH_{2m} nanocluster is a systematic process. For a given size, n, of the Mg_n cluster, we start the process of stepwise hydrogenation by adding two hydrogen atoms at a time. Two hydrogen atoms are added to the Mg_n cluster from various different directions and distances. Using symmetry unrestricted geometry optimizations at the 6-311+G(d,p) level, a large number of different Mg_nH_2 structures are obtained and compared. We can acquire the energetically lowest (second lowest, third lowest, etc.) structures. The best hydrogenated structure is considered to be the structure with the lowest energy and without imaginary frequencies. Based on the research results above, several low-lying Mg_nH_2 structures are selected as the bases of adding the second pair of hydrogen atoms. Subsequently, the best hydrogenated structure of Mg_nH_4 can be established. This process is repeated up to Mg_nH_{2n+2}. In order to consider the Mg_nH_{2m} geometry optimizations more completely, we also start adding or reducing a magnesium atom from the structures of $Mg_{n-1}H_{2m}$ or $Mg_{n+1}H_{2m}$. At last, the energetically lowest structures (at 6-311+G(d,p) level) in each case are further optimized at the aug-cc-pVDZ level with frequency calculations. In this study, we have calculated with the nanocluster size up to n = 9.

All the charges are analyzed by the Natural Bond Orbital (NBO) method in this study.[36,37]

2.2. Evaluating Energy of Clusters. For the energy of each Mg_n, $E(Mg_n)$; Mg_nH_{2m} nanocluster, $E(Mg_nH_{2m})$; and H_2 molecule, $E(H_2)$, the zero-point energy correction (ZPE) has been applied. Certainly, the systematic interest to the energy is the difference (not absolute energy). For the formation of the magnesium clusters, we consider the following proces. In this case, the binding energy for the magnesium clusters, $E_b(Mg_n)$, can be defined as follows:

$$nMg \rightarrow Mg_n$$

$$E_b(Mg_n) = E(Mg_n) - nE(Mg) \quad (1)$$

where $E(Mg)$ is the energy of one magnesium atom. We can also define the average binding energy for the magnesium clusters, $E_{ab}(Mg_n)$, as

$$E_{ab}(Mg_n) = \frac{E_b(Mg_n)}{n} = \frac{E(Mg_n)}{n} - E(Mg) \quad (2)$$

Similarly, we can also investigate the process for magnesium cluster formation from another aspect. In this case, we define the stepwise binding energy for the magnesium clusters, $E_{sb}(Mg_n)$, as follows:

$$Mg_{n-1} + Mg \rightarrow Mg_n$$

$$E_{sb}(Mg_n) = E(Mg_n) - E(Mg_{n-1}) - E(Mg) = E_b(Mg_n) - E_b(Mg_{n-1}) \quad (3)$$

The second differences of binding energy for magnesium clusters, $\Delta^2E_b(Mg_n)$, is as follows:

$$\Delta^2E_b(Mg_n) = E_b(Mg_{n+1}) + E_b(Mg_{n-1}) - 2E_b(Mg_n) \quad (4)$$

Similar to the formation of the Mg_n cluster, for a given size, n, of the Mg_n cluster, the H_2 molecules are adsorbed on it. This process is described as follows. Thus, the adsorption energy, $E_a(Mg_nH_{2m})$, and the average adsorption energy, $E_{aa}(Mg_nH_{2m})$, of the Mg_nH_{2m} nanoclusters are defined as

$$Mg_n + mH_2 \rightarrow Mg_nH_{2m}$$

$$E_a(Mg_nH_{2m}) = E(Mg_nH_{2m}) - E(Mg_n) - mE(H_2) \quad (5)$$

$$E_{aa}(Mg_nH_{2m}) = \frac{E_a(Mg_nH_{2m})}{m} = \frac{E(Mg_nH_{2m}) - E(Mg_n)}{m} - E(H_2) \quad (6)$$

Meanwhile, we could also consider a stepwise process. The stepwise adsorption energy for the Mg_nH_{2m} nanocluster, $E_{sa}(Mg_nH_{2m})$, is given as

$$Mg_nH_{2m-2} + H_2 \rightarrow Mg_nH_{2m}$$

$$E_{sa}(Mg_nH_{2m}) = E(Mg_nH_{2m}) - E(Mg_nH_{2m-2}) - E(H_2) \quad (7)$$

The basis set superposition error (BSSE), in this study, is very small and its influence can be neglected.[18]

To validate that the functional and the basis set which we select are reasonable for this study, the Mg−Mg bond length of the Mg_2 molecule, R(Mg−Mg), the H−H bong length of the H_2 molecule, R(H−H), and the energy of H_2 molecule, $E_{HF}(H_2)$, were calculated and compared with the experimental results (listed in Table 1). The calculated results, using B3PW91 functional with Grimme's dispersion correction and 6-311+G(d,p) or aug-cc-pVDZ basis set, were in good agreement with the experimental results, and we expected that the functional and the basis set selected were appropriate for our research.

3. RESULTS AND DISCUSSIONS

3.1. Determining the Global Minimum Structure for Mg_n Clusters. In our study, the "rough" global minimum state

DOI: 10.1021/acs.jpca.5b01474
J. Phys. Chem. A 2015, 119, 3636−3643

Table 1. Results Calculated at 6-311+G(d,p)/aug-cc-pVDZ +B3PW91(GD3) Level[a]

property	6-311+G(d, p)	aug-cc-pVDZ	experiments
R(Mg−Mg) (Å)	3.857	3.853	3.890[38]
R(H−H) (Å)	0.745	0.760	0.741
$E_{HF}(H_2)$ (a.u.)	−1.179	−1.174	−1.175

[a] R(Mg−Mg) represents the Mg−Mg bond length in a Mg_2 cluster. R(H−H) represents the H−H bong length in H_2 molecule. $E_{HF}(H_2)$ represents the energy of one H_2 molecule.

of each Mg_n cluster was initially determined using the "kick method" and further optimized with the more accurate method. The results of the cluster geometries were demonstrated in Figure 1, and the corresponding energies of the clusters are

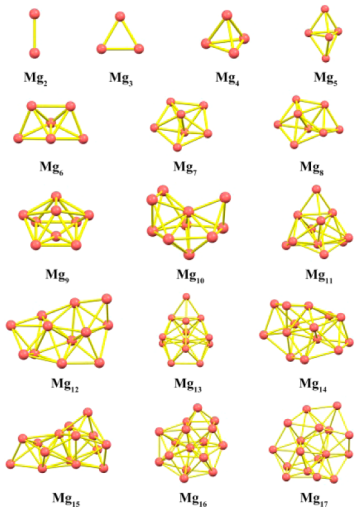

Figure 1. Optimized geometries of Mg_2−Mg_{17} clusters calculated at B3PW91 (D3 correction) + aug-cc-pVDZ level. One Mg atom is connected with its neighbor atoms with yellow sticks.

Table 2. Energies of Mg_2−Mg_{17} Clusters Calculated at B3PW91 (D3 Correction) + aug-cc-pVDZ Level

cluster size	energy (a.u.)	cluster size	energy (a.u.)
2	−400.0830	10	−2000.6083
3	−600.1395	11	−2200.6804
4	−800.2075	12	−2400.7430
5	−1000.2707	13	−2600.8282
6	−1200.3341	14	−2800.8954
7	−1400.4059	15	−3000.9460
8	−1600.4705	16	−3200.9986
9	−1800.5430	17	−3401.0792

listed in Table 2. Seeing Figure 1, we can find that the structure of the Mg_n cluster can be obtained from the structure of the Mg_{n-1} cluster adding one magnesium atom. This growth trend of the structure for the Mg_n cluster conforms to the "n+1" rule.[39]

Compared with previous results (Lyalinet al.[28] and Sandip De et al.[29]), the structure of the Mg_n cluster with n = 9 in this study is different. The structures of two Mg_9 clusters are shown in Figure 2.The obtained global minimum structure in this study (A) and previous study (B), the corresponding energies, and the HOMO−LUMO gap are also displayed.

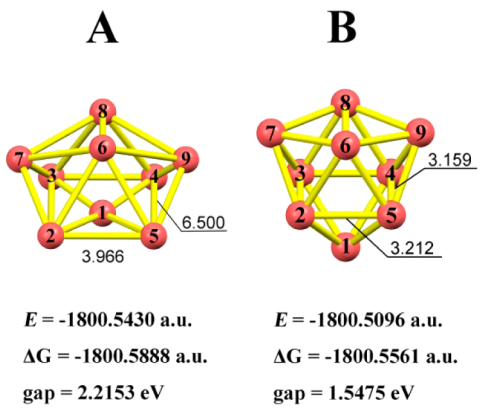

Figure 2. Global minimum structure of the Mg_9 cluster calculated in our study (A) and previous studies (B). One Mg atom is connected with its neighbor atoms with yellow sticks.

In Figure 2, Structure A shows lower zero-point energy and Gibbs free energy compared to structure B. The HOMO−LUMO gap of A is larger than that of B. These results mean that A is energetically lower and structurally more stable than B. The results of NBO analysis also support the above conclusion (see Table 3). The lower energy 3s orbitals are occupied by more electrons in A, but more electrons occupy the high-energy 3p orbits in B. It is also worth noting that, for structure A in Table 3, we find a special Mg atom (Mg1), which exhibits a relatively higher number of 3p electrons of 0.80. According to the geometric structure of this cluster (see Figure 2A), the Mg1 atom is positioned uniquely at the center of the 2, 3, 4, 5 rectangle. This may be the reason for the higher 3p occupancy and is discussed later in this section.

In order to describe the orbital delocalized degree of A and B, we selected localized orbital locator (LOL) function[40]

$$\mathrm{LOL} = \frac{\tau(\mathbf{r})}{1 + \tau(\mathbf{r})} \tag{8}$$

$$\tau(\mathbf{r}) = \frac{3}{5}(6\pi^2)^{2/3}\frac{[\rho^{\alpha}(\mathbf{r})^{5/3} + \rho^{\beta}(\mathbf{r})^{5/3}]}{\sum_i \eta_i |\nabla\varphi_i(\mathbf{r})|^2} \tag{9}$$

where ρ^{α} and ρ^{β} are the electron density with α and β spins. η_i is the orbital occupation, and φ_i is the molecular orbital. The LOL of A and B was plotted, using the *Multiwfn* software package (3.3.7 version)[41] as a function of Cartesian coordinates and projected onto a plane in Figure 3. Figure 3 shows the LOL of A and B in planes 2345, 256, and 186.

From the perspective of structure and bonding, we find that the distribution of LOL function value near the magnesium atom is not spherically symmetric in B (see Figure 3, each atom), and there is a region with higher localized degree between atoms (see Figure 3, yellow part). This explains that the magnesium atoms, through sp hybridization,[42−44] form normal two-center σ bonds (two-body interaction)[43] and three-center bonds (three-body interaction)[43] with other magnesium atoms. The NBO analysis also suggests that the orbital occupancies in 3s and 3p orbit are all close to 1, so that the magnesium atoms form a high-energy Mg_9 cluster (B) by sp hybridization. On the contrary, in A, the distribution of the LOL function value is spherically symmetric near the atoms (see Figure 3, each atom). Although 3s orbitals hybridize less with 3p orbitals (see Table 3, 3p orbital of A), it is not real sp hybridization because the orbitally localized degree is not very

DOI: 10.1021/acs.jpca.5b01474
J. Phys. Chem. A 2015, 119, 3636−3643

Table 3. Corresponding Natural Electron Configuration for Each Mg Atom in 3s and 3p Orbits[a]

	orbit	Mg1	Mg2	Mg3	Mg4	Mg5	Mg6	Mg7	Mg8	Mg9
A	3s	1.63	1.70	1.70	1.70	1.70	1.66	1.70	1.66	1.70
	3p	0.80	0.19	0.19	0.19	0.19	0.34	0.27	0.34	0.27
B	3s	1.24	1.20	1.20	1.20	1.20	1.20	1.24	1.20	1.24
	3p	0.69	0.79	0.79	0.79	0.79	0.79	0.69	0.79	0.69

[a]The structures and Mg sequences are shown in Figure 2.

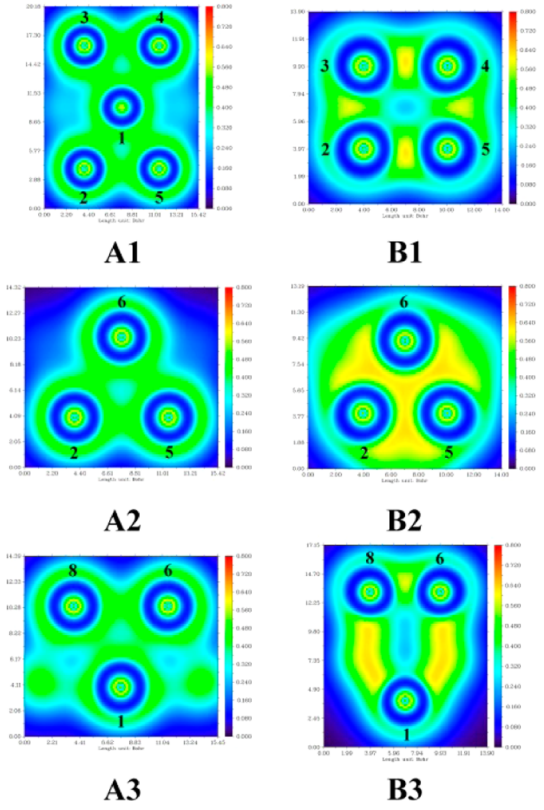

Figure 3. Distribution of LOL function values in the planes 2345, 256, and 186 of the Mg_9(A) and Mg_9(B). The numbers in the figure correspond to the atomic numbers of the magnesium atoms in Figure 2.

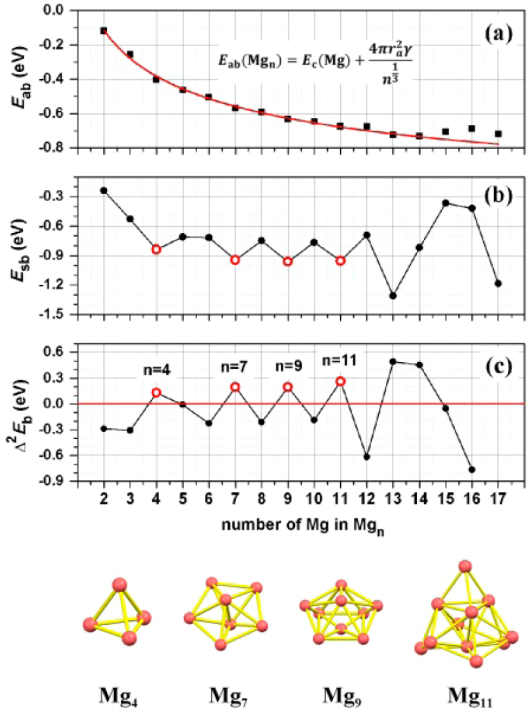

Figure 4. Average $[E_{ab}(Mg_n)]$ (a), stepwise $[E_{sb}(Mg_n)]$ (b), and second differences of $[\Delta^2 E_b(Mg_n)]$ (c) binding energy of the magnesium clusters as a function of cluster size. The structures of the stable structures for Mg_4, Mg_7, Mg_9, and Mg_{11} clusters are also displayed. Points in (a) are coupled with eq 10 (see red curve).

high in each region (see Figure 3, green part). The 3s orbitals of magnesium atoms overlap with each other to form a delocalized π bond, to form a lower energy Mg_9 cluster (A). By the above discussion, the Mg_9 cluster (A) we find in this study may be more stable in comparison with previous work.

3.2. Determining the Relatively Stable Mg_n Among All the Mg_n Clusters. The average binding energy, stepwise binding energy, and second differences of binding energy are all displayed in Figure 4. The exact values of these results are listed in the Supporting Information (Table S1) correspondingly. In Figure 4a, the absolute values of the average binding energies gradually increase with the growing cluster size. According to the liquid-drop model (LDM),[45] the binding energy of the cluster equals the total cohesive energy of the bulk $[E_c(Mg)]$ plus the surface energy (B). Hence, the average binding energy of the magnesium clusters, $E_{ab}(Mg_n)$, is given by[45]

$$E_{ab}(Mg_n) = E_c(Mg) + \frac{B}{n^{1/3}}$$

$$B = 4\pi r_a^2 \gamma \qquad (10)$$

where r_a is the radius of the magnesium atom, and γ is the surface tension. Thus, we fitted the data in Figure 4a with eq 10 (see Figure 4a, red curve). According to our calculation, $E_c(Mg) = -1.42$ eV, and B is 1.64 eV. When $n \to \infty$, the magnesium cluster becomes a magnesium bulk and $E_{ab}(Mg_n) = E_c(Mg)$ (−1.42 eV). This value is close to the experimental value of −1.51 eV[46] for the magnesium crystal. It is also noted that, in comparison to previous studies,[28] our calculations include the van der Waals (VdW) interaction in obtaining the global minimum structures of magnesium. This is because the electronic shells in the divalent atoms are filled $3s^2$.[28]

From Figure 4b, we can see that the tendency of the stepwise binding energy is oscillating with the increase of cluster size. This indicates the existence of relatively stable clusters. Considering $\Delta^2 E_b(Mg_n)$ vs cluster size n (see Figure 4c), the values of the second differences of binding energy of the Mg_4, Mg_7, Mg_9, and Mg_{11} clusters are above zero, while the other Mg_n clusters with n = 3, 5, 6, 8, 10, and 12 are all negative. This result reinforces our previous conclusion that the Mg_4, Mg_7, Mg_9, and Mg_{11} clusters are the relatively stable magnesium clusters. The structures of the Mg_4, Mg_7, Mg_9, and Mg_{11} clusters have been shown in Figure 4.[47]

DOI: 10.1021/acs.jpca.5b01474
J. Phys. Chem. A 2015, 119, 3636−3643

3.3. Determining the Chemisorption Geometry of Mg_4H_2. In order to determine the global minimum geometry of Mg_nH_{2m}, we start with the relatively simple cluster of Mg_4H_2. The Mg_4H_2 cluster is calculated with the "kick method" and the most stable chemisorption structure is displayed in Figure 5.

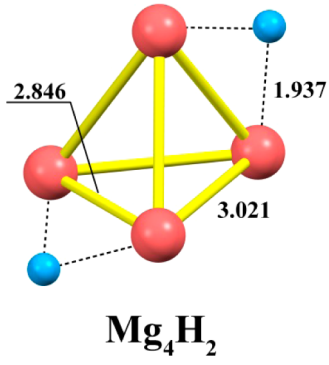

Figure 5. Obtained global minimum geometry of Mg_4H_2. Red and blue balls represent the magnesium and hydrogen atoms, respectively.

Compared to the Mg_4 cluster, the positions of Mg atoms are similar, while the Mg−Mg bond length has extended to 2.846 and 3.021 Å. The Mg−H bond length is found as 1.937 Å. This bond length is adopted as the typical chemisorption bond length and has been considered in building other Mg_nH_{2m} geometries.

According to previous studies, the strong physisorption energy of H_2 onto substrate is usually in the range of 0.1−0.3 eV. In this study, we also calculated the physisorption energy of H_2 molecules adsorbed onto Mg_4 clusters (up to Mg_4+3H_2). The structures and Cartesian coordinates of that are shown in Figure S1 and Table S2 in Supporting Information. The physisorption energy values for the first, second, and third H_2 are −0.038 eV, −0.044 eV, and −0.041 eV correspondingly. This indicates that the physisorption in our system is relatively weak and negligible.

3.4. Geometries and Energies of Mg_nH_{2m} Clusters. A systematic method has been applied to find the ground state geometry of Mg_nH_{2m} nanoclusters (see section 2). The calculated results of the Mg_nH_{2m} nanocluster geometries are demonstrated in Figure 6. The Cartesian coordinates and corresponding energies of the Mg_nH_{2m} nanoclusters are listed in Supporting Information Tables S3 and S4. For the adsorption of the first pair of hydrogens (Mg_nH_2), the hydrogen atoms distribute symmetrically in the Mg_n clusters. For all the structures, the original geometry of the Mg cluster has not been significantly changed.

The results of the stepwise and average adsorption energy for the Mg_nH_{2m} nanoclusters (see Section 2, eqs5−7) as a function of the number of hydrogen adsorbed are display in Figure 7 (n = 2−5, m = 2 ∼ n+1) and Figure 8 (n = 6−9, m = 2 ∼ n+1). The detailed values are given in Supporting Information Table S4. According to our results, all the energy curves exhibit a similar trend. The properties of Mg_n adsorbing hydrogen for different cluster sizes are consistent.

From the results of stepwise adsorption energies (Figures 7a and 8a), the stepwise adsorption energies [$E_{sa}(Mg_nH_{2m})$] for the first pair of hydrogens are all above zero, indicating an endothermic process. However, for the remaining pairs of hydrogen (m = 2, 3, ···, n), the stepwise $E_{sa}(Mg_nH_{2m})$ drops dramatically to the level below −0.3 eV. This indicates an exothermic chemisorption process, which means the hydrogen molecules are relatively inclined to be chemisorbed onto the Mg_nH_{2m-2} (m = 2, 3,···, n) cluster.

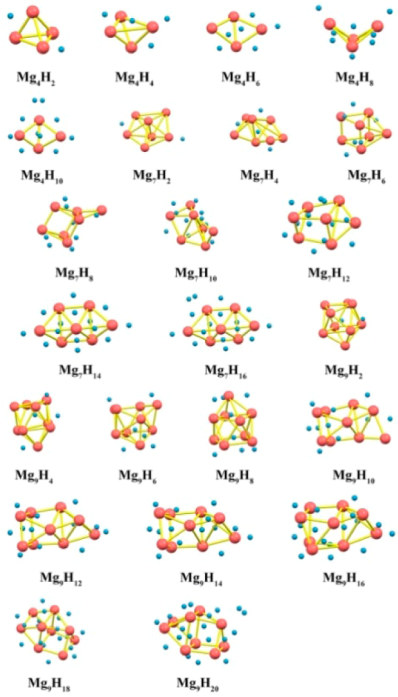

Figure 6. Optimized geometries of the Mg_nH_{2m} nanoclusters calculated in the B3PW91 functional with Grimme's dispersion correction at aug-cc-pVDZ level. Red balls represent the magnesium atoms and blue balls represent the hydrogen atoms.

It is also worth noting that when m = n, the calculated average adsorption Gibbs free energies for all the clusters are below zero (see Table 4), which means the formation of Mg_nH_{2m} can happen spontaneously. When the cluster sizes are relatively large (6−9), the Mg_nH_{2n} formed seems more stable. The next pair of hydrogens adsorbed (from Mg_nH_{2n} to Mg_nH_{2n+2}) shows $E_{sa}(Mg_nH_{2n+2})$ at around −0.1 eV (blue points in Figures 7a and 8a). This indicates that adding a pair of hydrogen atoms onto Mg_nH_{2n} is weak physical adsorption. Thus, the property of Mg_nH_{2n+2} is not considered in this study. In other words, the saturated state for hydrogen (chemical) adsorption should be Mg_nH_{2n}, which is the stoichiometry of the MgH_2 crystal (1:2).

For Figures 7b and 8b, the average adsorption energies [$E_{aa}(Mg_nH_{2m})$] have been steadily below −0.3 eV when m > 3. From Table 4, a stable chemisorbed Mg_nH_{2m} should be at least $n \geq 4$. An dramatic energy drop has been observed for the average adsorption energies [$E_{aa}(Mg_nH_{2m})$] (see Figures 7b, 8b). For all nanoclusters, the Mg_nH_{2n} nanoclusters (stoichiometric composition) are the most stable clusters composed by chemisorption. In this case, with the increasing the size, n, the Mg_nH_{2n} nanocluster will ultimately converge to MgH_2 bulk (or crystal). Thus, we may employ a smooth curve to describe the variation of the average adsorption energy of the Mg_nH_{2n} nanocluster, $E_{aa}(Mg_nH_{2n})$, with the size, n, and extrapolate that all the way to infinity. We fitted the energy data (see Figures 7b and 8b, orange points) to the function

$$E_{aa}(Mg_nH_{2n}) = E_0 + Ke^{-an} \quad (11)$$

DOI: 10.1021/acs.jpca.5b01474
J. Phys. Chem. A 2015, 119, 3636−3643

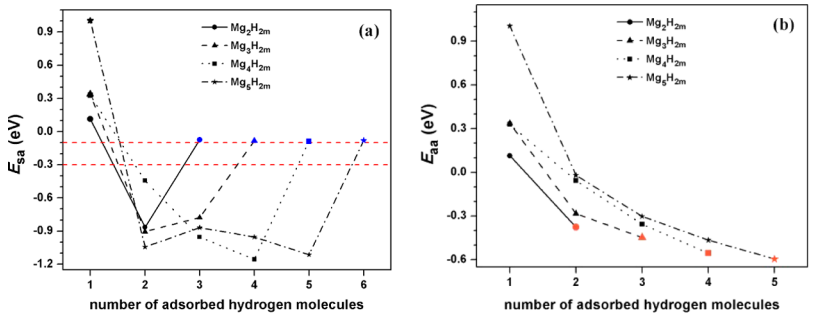

Figure 7. Stepwise adsorption energies $[E_{sa}(Mg_nH_{2m})]$ (a) and the average adsorption energies $[E_{aa}(Mg_nH_{2m})]$ (b) of the Mg_nH_{2m} nanoclusters as a function of the number of hydrogens adsorbed on magnesium cluster, m, with n = 2−5, m = 2 ∼ n+1.

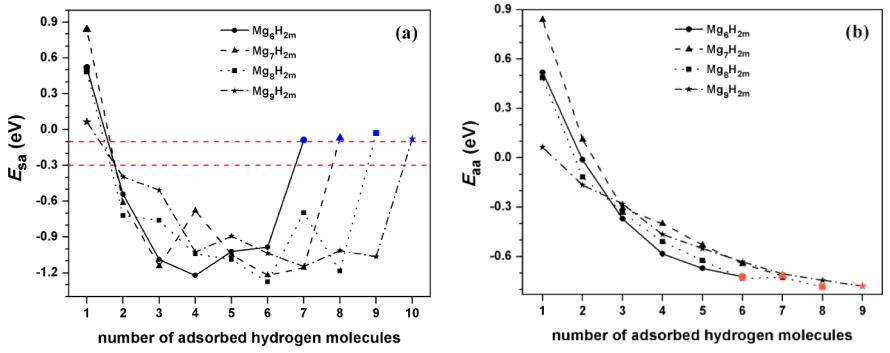

Figure 8. Stepwise adsorption energies $[E_{sa}(Mg_nH_{2m})]$ (a) and the average adsorption energies $[E_{aa}(Mg_nH_{2m})]$ (b) of the Mg_nH_{2m} nanoclusters as a function of the number of hydrogens adsorbed on the magnesium cluster, m, with n = 6−9, m = 2 ∼ n+1.

Table 4. Average Gibbs Free Energy for the Formation of Mg_nH_{2n} Nanoclusters

clusters	Mg_2H_4	Mg_3H_6	Mg_4H_8	Mg_5H_{10}	Mg_6H_{12}	Mg_7H_{14}	Mg_8H_{16}	Mg_9H_{18}
ΔG_{aa} (eV)	−0.11	−0.15	−0.26	−0.29	−0.41	−0.41	−0.46	−0.47

According to our fitting (see Figure 9, blue curve), E_0 = −0.818 eV, K = 0.882 eV, and α = 0.315. When $n \rightarrow \infty$, then

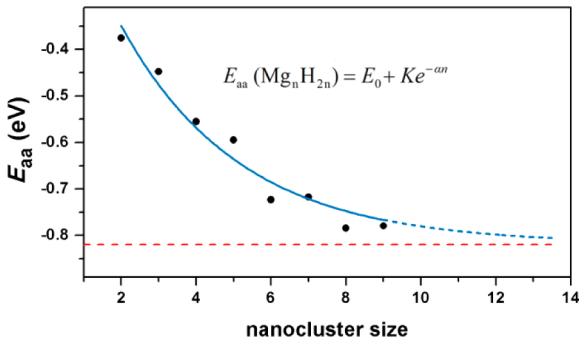

Figure 9. Average adsorption energy of the Mg_nH_{2n} cluster, $E_{aa}(Mg_nH_{2n})$, in kJ/mol. The points are coupled with eq 11 (see blue curve and blue dashed curve). The average adsorption energy for the Mg_nH_{2n} nanocluster (−0.818 eV, −78.987 kJ/mol) gradually converges to the red dashed line.

Mg_nH_{2n} nanocluster → MgH_2 crystal and $E_{aa}(Mg_nH_{2n}) \rightarrow E_0$ = −0.818 eV (−78.987 kJ/mol) (see Figure 9, blue dashed curve). This value is close to the experimental value of −75.3 kJ/mol[48] of the MgH_2 crystal.

According to our previous analysis, the first and second pairs of hydrogen are not thermodynamically favorable, while the chemisorption process become favored after the third pair of hydrogen. This may indicate that the combination of Mg and H_2 depends on the sufficient mix of two components. The simulation result is also consistent with the experiment which shows that there may exist a substoichiometric nanostructured phase of MgH_x hydride ($x < 2$) in a ball-milled nanostructure of MgH_2[24] and the hydrogen, in this phase, could diffuse much more rapidly.[23] Thus, it is possible to design a nanostructure of Mg_nH_{2m} hydride ($n \geq 4$, $3 \leq m < n$) for easy hydrogen storage.

3.5. Regulation of Mg_nH_{2m} Average Adsorption Energy. To this end, we attempted to describe the dependence of average adsorption energy, $E_{aa}(Mg_nH_{2m})$ as the function of m and n. For a given Mg_nH_{2m} cluster, we suppose the $E_{aa}(Mg_nH_{2m})$ can be expressed in the following form:

$$E_{aa}(Mg_nH_{2m}) = f(n, m) + E_{aa}(Mg_nH_{2n}) \quad (m = 1, 2, 3, ..., n) \tag{12}$$

In a certain Mg_nH_{2m} cluster, the energy difference between the fully absorbed state (Mg_nH_{2n}) and other states (Mg_nH_{2m}) is solely described as a function of n and m. In order to separate m and n, we extrapolate $f(n, m)$ as $f(n, x)$ where x equals m/n. We separate variables in $f(n, x)$ and couple the curve according to the results in Figures 7b and 8b (see Supporting Information Section 5)

$$f(n, x) = A(n)\, e^{4(1-x)} - C \tag{13}$$

where $A(n)$ is only the function of n. C is a constant. It should also be noted that when $m = n$ we have $x = 1$ and $f(n, x) = 0$. Thus

DOI: 10.1021/acs.jpca.5b01474
J. Phys. Chem. A 2015, 119, 3636−3643

$$C = A(n) \tag{14}$$

More details for this simulation are given in the Supporting Information. Taking eqs 11, 13, 14 into 12, we get the following expression:

$$E_{aa}(Mg_nH_{2m}) = A(n)[e^{4(1-x)} - 1] + E_0 + K\, e^{-\alpha n}$$
$$(x = m/n,\ m = 1, 2, 3, ..., n) \tag{15}$$

Our result shows that for one Mg_n cluster, the hydrogen adsorption capability solely depends on the cluster size n and the ratio of x in MgH_{2x}. This equation may be applied in evaluating the chemisorption capability for Mg_n or other clusters (metallic or nonmetallic). It is also noted that due to the limitation of our data, the form of $A(n)$ has not been fitted. This can be fixed in further studies.

4. CONCLUDING REMARKS

The global minimum states of Mg_n clusters with the cluster sizes up to 17 are determined with the "kick method". According to our calculation, the "kick method" is effective to explore the global minimum state of clusters. In this study, we find a global minimum state of Mg_9 cluster which is more stable than previous work. Furthermore, we obtain the size dependence of the average binding energy for Mg_n cluster.

Through the investigation on hydrogen storage in Mg_n clusters, we find that as the Mg_n cluster adsorbs a pair of hydrogen, the (stepwise) adsorption energies are larger than zero. However, as more hydrogen is adsorbed on the Mg_n cluster, the (stepwise) adsorption energies are below zero because the hydrogen can fully come into contact with the Mg_n cluster from various directions. When the number of adsorbed hydrogens m is up to n, the next pair of hydrogens adsorbed shows low (stepwise) adsorption energies. It means that the saturated state for hydrogen chemisorption should be Mg_nH_{2n}, which is the stoichiometry of the MgH_2 crystal. At last, we construct the dependence of average adsorption energy for the Mg_nH_{2m} nanocluster on the size (n) and composition (m). Our calculation results and coupled functions may be extrapolated to other gas-cluster chemisorption circumstance. Further studies based on both experimental and theoretical are welcome to verify the results.

■ ASSOCIATED CONTENT

Supporting Information

Binding energies, structures, and Cartesian coordinates. This material is available free of charge via the Internet at http://pubs.acs.org.

■ AUTHOR INFORMATION

Corresponding Author

*E-mail: zhanghx@jlu.edu.cn.

Notes

The authors declare no competing financial interest.

■ ACKNOWLEDGMENTS

We would like to thank Natural Science Foundation of China (Grant No. 21173096, No. 21303068, No. 21273095) and Research Fund for the Doctoral Program of Higher Education of China (No. 20130061120025) for the support of this work.

■ REFERENCES

(1) Graetz, J. New Approaches to Hydrogen Storage. *Chem. Soc. Rev.* **2009**, *38*, 73−82.
(2) Schlapbach, L.; Zuttel, A. Hydrogen-Storage Materials for Mobile Applications. *Nature* **2001**, *414*, 353−358.
(3) Züttel, A. Materials for Hydrogen Storage. *Mater. Today* **2003**, *6*, 24−33.
(4) Jain, I. P. Hydrogen the Fuel for 21st Century. *Int. J. Hydrogen Energy* **2009**, *34*, 7368−7378.
(5) Dillon, A. C.; Jones, K. M.; Bekkedahl, T. A.; Kiang, C. H.; Bethune, D. S.; Heben, M. J. Storage of Hydrogen in Single-Walled Carbon Nanotubes. *Nature* **1997**, *386*, 377−379.
(6) Li, H.; Eddaoudi, M.; O'Keeffe, M.; Yaghi, O. M. Design and Synthesis of an Exceptionally Stable and Highly Porous Metal-Organic Framework. *Nature* **1999**, *402*, 276−279.
(7) Rosi, N. L.; Eckert, J.; Eddaoudi, M.; Vodak, D. T.; Kim, J.; O'Keeffe, M.; Yaghi, O. M. Hydrogen Storage in Microporous Metal-Organic Frameworks. *Science* **2003**, *300*, 1127−1129.
(8) Manchester, F. D.; San-Martin, A.; Pitre, J. M. The H-Pd (Hydrogen-Palladium) System. *J. Phase Equilib.* **1994**, *15*, 62−83.
(9) Sandrock, G. A Panoramic Overview of Hydrogen Storage Alloys from a Gas Reaction Point of View. *J. Alloys Compd.* **1999**, *293*−*295*, 877−888.
(10) Graetz, J.; Reilly, J. J.; Kulleck, J. G.; Bowman, R. C. Kinetics and Thermodynamics of the Aluminum Hydride Polymorphs. *J. Alloys Compd.* **2007**, *446*−*447*, 271−275.
(11) Zhang, X.-Q.; Iype, E.; Nedea, S. V.; Jansen, A. P. J.; Szyja, B. M.; Hensen, E. J. M.; van Santen, R. A. Site Stability on Cobalt Nanoparticles: A Molecular Dynamics ReaxFF Reactive Force Field Study. *J. Phys. Chem. C* **2014**, *118*, 6882−6886.
(12) Orimo, S.-i.; Nakamori, Y.; Eliseo, J. R.; Züttel, A.; Jensen, C. M. Complex Hydrides for Hydrogen Storage. *Chem. Rev.* **2007**, *107*, 4111−4132.
(13) Bogdanović, B.; Sandrock, G. Catalyzed Complex Metal Hydrides. *MRS Bull.* **2002**, *27*, 712−716.
(14) Grant, A. W.; Ngo, L. T.; Stegelman, K.; Campbell, C. T. Cyclohexane Dehydrogenation and H_2 Adsorption on Pt Particles on ZnO(0001)−O. *J. Phys. Chem. B* **2003**, *107*, 1180−1188.
(15) Makowski, P.; Thomas, A.; Kuhn, P.; Goettmann, F. Organic Materials for Hydrogen Storage Applications: from Physisorption on Organic Solids to Chemisorption in Organic Molecules. *Energy Environ. Sci.* **2009**, *2*, 480−490.
(16) Sakintuna, B.; Lamari-Darkrim, F.; Hirscher, M. Metal Hydride Materials for Solid Hydrogen Storage: A Review. *Int. J. Hydrogen Energy* **2007**, *32*, 1121−1140.
(17) Wagemans, R. W. P.; van Lenthe, J. H.; de Jongh, P. E.; van Dillen, A. J.; de Jong, K. P. Hydrogen Storage in Magnesium Clusters: Quantum Chemical Study. *J. Am. Chem. Soc.* **2005**, *127*, 16675−16680.
(18) Koukaras, E. N.; Zdetsis, A. D.; Sigalas, M. M. Ab initio Study of Magnesium and Magnesium Hydride Nanoclusters and Nanocrystals: Examining Optimal Structures and Compositions for Efficient Hydrogen Storage. *J. Am. Chem. Soc.* **2012**, *134*, 15914−15922.
(19) Cheng, F.; Tao, Z.; Liang, J.; Chen, J. Efficient Hydrogen Storage with the Combination of Lightweight Mg/MgH_2 and Nanostructures. *Chem. Commun.* **2012**, *48*, 7334−7343.
(20) Norberg, N. S.; Arthur, T. S.; Fredrick, S. J.; Prieto, A. L. Size-Dependent Hydrogen Storage Properties of Mg Nanocrystals Prepared from Solution. *J. Am. Chem. Soc.* **2011**, *133*, 10679−10681.
(21) Zaluska, A.; Zaluski, L.; Ström−Olsen, J. O. Nanocrystalline Magnesium for Hydrogen Storage. *J. Alloys Compd.* **1999**, *288*, 217−225.
(22) Jeon, K.-J.; Moon, H. R.; Ruminski, A. M.; Jiang, B.; Kisielowski, C.; Bardhan, R.; Urban, J. J. Air-Stable Magnesium Nanocomposites Provide Rapid and High-Capacity Hydrogen Storage without Using Heavy-Metal Catalysts. *Nat. Mater.* **2011**, *10*, 286−290.
(23) Varin, R. A.; Czujko, T.; Wronski, Z. Particle Size, Grain Size and γ-MgH_2 Effects on the Desorption Properties of Nanocrystalline Commercial Magnesium Hydride Processed by Controlled Mechanical Milling. *Nanotechnology* **2006**, *17*, 3856.

DOI: 10.1021/acs.jpca.5b01474
J. Phys. Chem. A 2015, 119, 3636−3643

(24) Schimmel, H. G.; Huot, J.; Chapon, L. C.; Tichelaar, F. D.; Mulder, F. M. Hydrogen Cycling of Niobium and Vanadium Catalyzed Nanostructured Magnesium. *J. Am. Chem. Soc.* **2005**, *127*, 14348−14354.
(25) Roy, D.; Corminboeuf, C.; Wannere, C. S.; King, R. B.; Schleyer, P. v. R. Planar Tetracoordinate Carbon Atoms Centered in Bare Four-Membered Rings of Late Transition Metals. *Inorg. Chem.* **2006**, *45*, 8902−8906.
(26) Bera, P. P.; Sattelmeyer, K. W.; Saunders, M.; Schaefer, H. F.; Schleyer, P. v. R. Mindless Chemistry. *J. Phys. Chem. A* **2006**, *110*, 4287−4290.
(27) Saunders, M. Stochastic Search for Isomers on a Quantum Mechanical Surface. *J. Comput. Chem.* **2004**, *25*, 621−626.
(28) Lyalin, A.; Solov'yov, I. A.; Solov'yov, A. V.; Greiner, W. Evolution of the Electronic and Ionic Structure of Mg Clusters with Increase in Cluster Size. *Phys. Rev. A* **2003**, *67*, 063203.
(29) De, S.; Ghasemi, S. A.; Willand, A.; Genovese, L.; Kanhere, D.; Goedecker, S. The Effect of Ionization on the Global Minima of Small and Medium Sized Silicon and Magnesium Clusters. *J. Chem. Phys.* **2011**, *134*, 124302.
(30) Hohenberg, P.; Kohn, W. Inhomogeneous Electron Gas. *Phys. Rev.* **1964**, *136*, B864−B871.
(31) Kohn, W.; Sham, L. J. Self-Consistent Equations Including Exchange and Correlation Effects. *Phys. Rev.* **1965**, *140*, A1133−A1138.
(32) Becke, A. D. Density-Functional Exchange-Energy Approximation with Correct Asymptotic Behavior. *Phys. Rev. A* **1988**, *38*, 3098−3100.
(33) Perdew, J. P.; Chevary, J. A.; Vosko, S. H.; Jackson, K. A.; Pederson, M. R.; Singh, D. J.; Fiolhais, C. Atoms, Molecules, Solids, and Surfaces: Applications of the Generalized Gradient Approximation for Exchange and Correlation. *Phys. Rev. B* **1992**, *46*, 6671−6687.
(34) Grimme, S.; Antony, J.; Ehrlich, S.; Krieg, H. A Consistent and Accurate ab initio Parametrization of Density Functional Dispersion Correction (DFT-D) for the 94 Elements H-Pu. *J. Chem. Phys.* **2010**, *132*, 154104.
(35) Tong, J.; Li, Y.; Wu, D.; Li, Z.-R.; Huang, X.-R. Low Ionization Potentials of Binuclear Superalkali B2Li11. *J. Chem. Phys.* **2009**, *131*, 164307.
(36) Reed, A. E.; Curtiss, L. A.; Weinhold, F. Intermolecular Interactions from a Natural Bond Orbital, Donor-Acceptor Viewpoint. *Chem. Rev.* **1988**, *88*, 899−926.
(37) Bader, R. F. W. A Quantum Theory of Molecular Structure and Its Applications. *Chem. Rev.* **1991**, *91*, 893−928.
(38) Huber, K. P.; Herzberg, G. *Molecular Spectra and Molecular Structure IV. Constants of Dlatomic Molecules*; Van Nostrand Reinhold: New York, 1979.
(39) Wei, S. H.; Zeng, Z.; You, J. Q.; Yan, X. H.; Gong, X. G. A Density-Functional Study of Small Titanium Clusters. *J. Chem. Phys.* **2000**, *113*, 11127−11133.
(40) Schmider, H. L.; Becke, A. D. Chemical Content of the Kinetic Energy Density. *J. Mol. Struct.: THEOCHEM* **2000**, *527*, 51−61.
(41) Lu, T.; Chen, F. Multiwfn: A Multifunctional Wavefunction Analyzer. *J. Comput. Chem.* **2012**, *33*, 580−592.
(42) Bauschlicher, C. W.; Bagus, P. S.; Cox, B. N. On Hybridization and Bonding in the Alkaline Earths: Be, Mg, and Ca. *J. Chem. Phys.* **1982**, *77*, 4032−4038.
(43) Kaplan, I. G.; Roszak, S.; Leszczynski, J. Nature of Binding in the Alkaline−Earth Clusters: Be3,Mg3, and Ca3. *J. Chem. Phys.* **2000**, *113*, 6245−6252.
(44) Walch, S. P.; Bauschlicher, C. W. On 3d Bonding in the Transition Metal Trimers: The Electronic Structure of Equilateral Triangle Ca3, Sc3, Sc+3, and Ti+3. *J. Chem. Phys.* **1985**, *83*, 5735−5742.
(45) Vanithakumari, S. C.; Nanda, K. K. Phenomenological Predictions of Cohesive Energy and Structural Transition of Nanoparticles. *J. Phys. Chem. B* **2005**, *110*, 1033−1037.
(46) Kittel, C. *Introduction to Solid State Physics*, 8th ed. (in Chinese); Chemical Industry Press: Beijing, China, 2010.
(47) Ekardt, W. *Metal Clusters*; Wiley: New York, 1999.
(48) Dean, J. A. *Lange's Handbook of Chemistry*, 15th ed. (in Chinese); Science Publisher: Beijing, China, 2003.

DOI: 10.1021/acs.jpca.5b01474
J. Phys. Chem. A 2015, 119, 3636−3643